Vol. 08, No. 2 (2026) 1377-1388, doi: 10.24874/PES08.02B.026

Proceedings on Engineering Sciences

www.pesjournal.net

PRODUCTION OF CHRYSOTILE ASBESTOS FIBER REINFORCED GEOPOLYMER BRICKS

Zvikomborero Lazarus Duri[1]
Rajesh Arora
Naveen BP
Q.C. Kanhukamwe

Received 03.02.2026.
Revised 28.05.2026.
Accepted 13.06.2026.

Keywords:

Chrysotile asbestos, Geopolymer cement, Mix design, High speed mixer, Rheology

A B S T R A C T

Clay and pozzolanic materials of different grades were mined and processed by first crushing them and then grinding them as raw materials to very fine powders. These powders were then calcined separately at different temperature levels ranging from 550 degrees Celsius to 850 degrees Celsius. The materials were also characterised before and after pyro processing using the XRF, XRD and PSD. One molar solution of Na OH and KOH were prepared and mixed with various proportions of the geopolymer materials. Chrysotile asbestos fibres of different furnish designs were also prepared. These fibres which provide reinforcement to the geopolymer are then mixed with the various grades of geopolymer materials according to the chosen mix designs. The resulting mix design is then first passed through a slow speed mixer and then through a high-speed mixer. The rheology of the product gradually changed from being a dry powder to be a liquid paste after mixing at high speed with the chrysotile fibre providing the reinforcement. The liquid paste was then used to produce bricks using a vibration mechanism and the top moving part of the brick making machine as the compaction mechanism. Properties of the chrysotile fibre reinforced bricks were tested at 2 days, 7days, 14 days and 28days for compressive strengths, tensile strengths, corrosion resistance and resistance to acid attack. The results of the asbestos fibre reinforced geopolymer cement bricks were found to have improved properties with regards to compressive strengths, tensile strengths, corrosion resistance and resistance to acid attack when compared to ordinary cement concrete bricks..

1. INTRODUCTION

Different Geopolymer inputs have different physical and chemical characteristics depending on source or process from which they are made (Lyon et al., 1997) (Davidovits, 1991). High physical and chemical quality variability of materials even from the same source were noticed due to variations within raw material sources (Abd Elaty et al., 2014). Different grindability of materials means different particle sizes for various materials in same product after grinding (Duxson et al., 2006). Current Pyro-processing and Grinding process has limitations to achieve same particle size after grinding for optimized chemical reaction (Wang et al., 2005). Product strength/Quality can only be determined after hydration. – which is a destructive testing technique. Current

[1] Corresponding author: Zvikomborero Lazarus Duri
Email: lazarus@rulethu.com

manufacturing process or system has a poor response to rapid changes in raw material quality and process conditions (Abd Elaty et al., 2014). Current manufacturing processes producing product that is economically incompetent and is only used for specialised applications (Lyon et al, 1997) (Palomo et al., 1999), (Provis & Van Deventer, 2009). Poor Early Day Strength Statistical Compliance and product rejection by structural engineers despite having better characteristics after 28 Days of natural curing. (Yeh, 2006).

The present study set out to address these limitations by treating the production of chrysotile asbestos fibre reinforced geopolymer bricks as a two-stage optimisation problem. The first stage optimised the comminution of the raw materials so that a uniform, highly reactive feed powder could be produced consistently, while the second stage optimised the mix design, mixing regime and curing conditions of the finished brick. Response surface methodology was used throughout so that the individual and combined effects of the controlling variables could be quantified and the optimum operating window identified.

2. MATERIALS AND METHODS

Clay and pozzolanic source materials of different grades were mined, crushed and milled to fine powders to serve as the geopolymer raw materials. Each material was calcined separately at temperatures ranging from 550 degrees Celsius to 850 degrees Celsius in order to dehydroxylate the clay phases and develop the reactive amorphous alumino-silicate content required for geopolymerisation. The materials were characterised both before and after pyro-processing using X-ray fluorescence (XRF) for bulk oxide composition, X-ray diffraction (XRD) for mineralogy and amorphous content, and particle size distribution (PSD) analysis for fineness. Because the constituent materials differ in grindability, controlling the fineness of each feed independently was necessary to achieve a comparable reacting particle size in the blended product.

A one molar (1 M) solution of sodium hydroxide (NaOH) and, separately, of potassium hydroxide (KOH) was prepared to act as the alkaline activator and was combined with the geopolymer powders in the proportions fixed by each mix design. Chrysotile asbestos fibres of several furnish designs were prepared to provide reinforcement and were blended with the various grades of geopolymer material according to the chosen mix designs. The blended charge was first homogenised in a low-speed mixer running at approximately 30 revolutions per minute, which allowed the geopolymer reaction to initiate in the presence of the activator as the charge changed progressively from a dry powder to a semi-dry condition. The semi-dry paste was then transferred to a high-speed mixer operating at 980 revolutions per minute, where the rheology developed from a damp solid into a workable liquid paste and the chrysotile fibres became uniformly dispersed. Water of hydration liberated from the solid particles during high-speed mixing reported as free water once the paste was allowed to settle.

The reinforced liquid paste was cast into brick pre-forms using a machine that combined vibration with compaction from the descending upper platen, and the green bricks were demoulded and cured at a controlled temperature. Two brick profiles were prepared, one with a curved face for corners and bends and one with a straight face; the data reported here were obtained from the straight-face profile. Specimens were tested at 2, 7, 14 and 28 days for compressive strength, tensile strength, thermal response, corrosion resistance and resistance to acid attack, and benchmarked against ordinary cement concrete bricks.

Two experimental programmes were carried out within a response surface framework. The first programme optimised the grinding stage and examined two responses, the specific surface area of the milled powder and the grinding residue retained on the control sieve, against four grinding and feed-conditioning variables designated factors A to D. The second programme optimised brick production and examined the brick properties against six variables designated factors A to F, namely fibre content, NaOH concentration, geopolymer cement content, initial (low-speed) mixing time, final (high-speed) mixing time and curing temperature. In every case the high level of a factor was coded as +1 and the low level as -1. For each response a sequential model fit was performed and the best supported polynomial was selected on the basis of its sequential p-value, lack-of-fit p-value and adjusted and predicted coefficients of determination.

3. EXPERIMENTS

Experiment 1: Optimisation of Raw Material Grinding

The grinding responses were modelled first because the fineness and uniformity of the feed powders set the reactivity that is available to the downstream brick process. Specific surface area governs the rate and completeness of the alumino-silicate dissolution that drives geopolymerisation, whereas the residue retained on the control sieve quantifies the coarse, under-ground fraction that does not react fully and that tends to act as an inert filler in the hardened product (Table 1).

Table 1. Response 1: Surface Area. Fit Summary for Response 1: Surface Area

Source	Sequential p-value	Adjusted R^2
Linear	0.0006	0.4520
2FI	0.7139	0.3966
Quadratic	0.0043	0.9367
Cubic	0.2178	0.7976

The fit summary identifies the quadratic model as the best descriptor of specific surface area, returning a sequential p-value of 0.0043 and an adjusted R-squared of 0.9367. This is a marked improvement over the linear (0.4520) and two-factor interaction (0.3966) models, while the cubic model was found to be aliased by the design and was therefore not adopted. The reduced quadratic model for surface area is given in Equation 1.

$$\begin{aligned} Surface\ area\ = \ & 4129.90 + 345.83A - 511.67B \\ & + 449.61C - 425.00D \\ & + 205.06AB + 115.94AC \\ & + 178.94AD - 24.69BC \\ & + 60.56BD + 183.94CD \\ & + 662.19A2 + 274.69B2 \\ & + 379.19C2 \\ & - 357.31D2 \end{aligned} \quad (1)$$

The model shows that surface area responds most strongly to the curvature terms, in particular the positive quadratic coefficients of factor A (+662.19) and factor C (+379.19), which indicates that fineness is maximised towards the upper end of the studied range for these factors. Factor B carries a strong negative linear coefficient (-511.67), so raising it coarsens the powder, while factor D has a negative linear coefficient (-425.00) and a negative quadratic term, showing that excessive D reduces fineness, consistent with over-charging the mill and cushioning the grinding media. Because a higher surface area accelerates the dissolution that initiates geopolymerisation, the grinding window was set to favour the high-fineness region predicted by the model.

Table 2. Response 1: Surface Area. Fit Summary for Response 1: Surface Area

Source	Sequential p-value	Lack of Fit p-value	Adjusted R^2	Predicted R^2
Linear	0.0028	0.1043	0.3785	0.2769
2FI	0.7618	0.0757	0.3038	-0.2142
Quadratic	0.0963	0.1173	0.4621	-0.1362
Cubic	0.9813	0.0127	0.0613	-24.4267

For the grinding residue the linear model was the suggested model, with a sequential p-value of 0.0028, an adjusted R-squared of 0.3785 and a positive predicted R-squared of 0.2769 (Table 2). The higher-order models added no useful predictive power; the two-factor interaction and quadratic models both returned negative predicted R-squared values, which signals over-fitting, and the cubic model was aliased. The linear model for the residue is given in Equation 2.

$$\begin{aligned} & Residue \\ & = 10.83 - 2.72A + 3.50B - 2.00C \\ & + 3.33D \end{aligned} \quad (2)$$

The residue moves in the opposite sense to the surface area, as would be expected on physical grounds. Factors A and C, which increase fineness, reduce the coarse residue, with coefficients of -2.72 and -2.00 respectively, while factors B and D increase it, with coefficients of +3.50 and +3.33. The consistency in sign between the two grinding responses is important: it confirms that a single set of grinding conditions, favouring high levels of A and C and low levels of B and D, simultaneously maximises surface area and minimises residue. This yields a uniform, fully reactive feed powder, which directly addresses the variability and inconsistent particle size that were identified as limitations of the conventional process.

Experiment 2: Production and Testing of Geopolymer Bricks

The optimised feed powders were then carried forward into the brick production programme. The six-factor design matrix and the corresponding measured responses are summarised in Table 1, and the fitted models for each brick property, together with their fit summaries, are presented in the sections that follow. Across all of the brick responses the geopolymer cement content (factor C) and the alkali concentration (factor B) emerged as the dominant linear effects, with the fibre content (factor A) providing the principal reinforcement contribution to the strength responses.

The effects of cement, NaOH, mixing time and curing time on compressive strength are illustrated in the experimental data (Table 3, see Appendix).

The effects of cement, NaOH, mixing time and curing time on compressive strength.

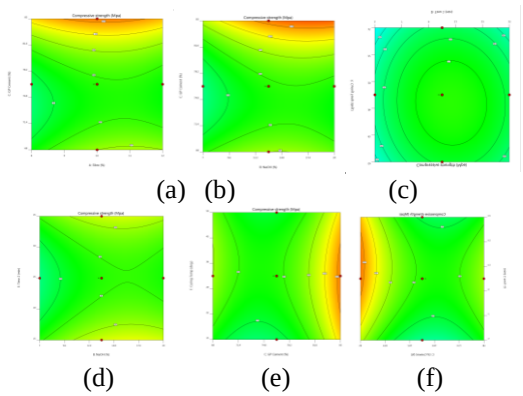

(a) (b) (c)

(d) (e) (f)

Figure 1. 2d Surface Responses for Compressive Strength

Figure 1(a) shows the response of compressive strength to Variations to cement and fibre content. Optimized strength is achieved when cement percentage increases together with a fibre content increase. However,

increases of fibre content up to 12% after which strength begins to decrease.

Figure 1(b) shows variations of compressive strength with variations of NaOH and cement content. Optimal performance when NaOH increases up to 20% above which the strength starts to come down. Low levels of NaOH also lead to inadequate cement activation which result in low compressive strength development.

Figure 1(c) shows the effect of mixing time and curing temperature on compressive strength. An initial mixing time of 15 minutes at a slow speed is required followed by a high speed mixing of 25 minutes to achieve maximum compressive strength on the Geopolymer brick.

Figure 1(d) shows the effect of mixing time and NaOH on compressive strength. A combination of 15 minutes slow speed mixing and 20 minutes of high speed mixing produces maximum strength when up to a maximum of 20% NaOH (alkali) is used.

Figure 1(e) shows the relationship of compressive strength to variations of cement and curing temperature. Maximum compressive strength is achieved when 85% cement is used together with a curing temperature of 50 degrees. Higher temperatures above that will result in reduced strength due to excessive dehydration of the alkali (NaOH) and lower temperatures result in a reduced initial activation threshold resulting in poor strength development between the cement and fibre bonds.

Figure 1(f) shows the relationship between compressive strength and mixing time. Maximum strength of cement is achieved when both high speed and low speed mixing times are below 25 minutes and also when cement percentages increase up to 85%. Higher mixing times result in the breaking up of compressive strength bonds or the cement fibre bonds once the activation process has been started.

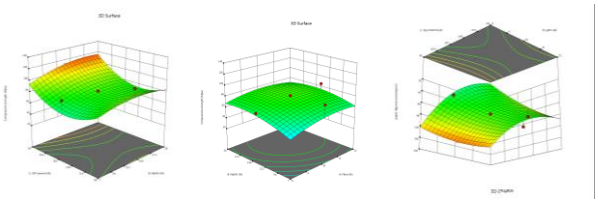

(a) (b) (c)

Figure 2. 3d Responses for Compressive Strength

Figure 2(a) shows the 3d surface response of compressive strength due to variations in cement and NaOH.

Low cement percentages result in lower strengths whilst NaOH percentages vary from 7 to 20%. Maximum strength is obtained when 12% fibre is mixed with 20% NaOH.
Figure 2(b) shows the impact of compressive strength due to variations of fibre and NaOH. 7% fibre produced the lowest results whilst 20% fibre produced the highest results. NaOH concentrations less than 7% are inadequate for Initial cement hydration process causing quick sets or a false sets whilst percentages greater than 20% causes rapid setting. Quick sets, false sets and rapid sets are not desirable for optimized compressive strength development as they lead to the formation of weak bonds.

Figure 2(c) shows the variation of compressive strength due to variations in fibre and cement. Fibre content above 20% results in reduced strengths due to inadequate/lower cement compositions as the fibre displaces the cement. Fibre content below 7% causes inadequate reinforcement.

4. SYSTEM EQUATION

4.1 Final Equation in Terms of Coded Factors

$$\begin{aligned} &Tensile\ Strength \\ &= 14.77 + 1.14A + 1.39B + 1.97C + 0.9242D \\ &- 0.1061E + 0.6212F - 0.5312AB - 0.7187AC \\ &+ 0.2813AD + 0.2812AE - 0.3125AF + 0.8125BC \\ &- 0.4375BD - 0.4375BE - 0.4063BF + 0.3750CD \\ &- 0.3750CE - 0.7188CF + 0.6875DE + 0.4062DF \\ &+ 0.4063EF\ . \end{aligned} \quad (3)$$

The equation in terms of coded factors can be used to make predictions about the response for given levels of each factor. By default, the high levels of the factors are coded as +1 and the low levels are coded as -1. The coded equation is useful for identifying the relative impact of the factors by comparing the factor coefficients.

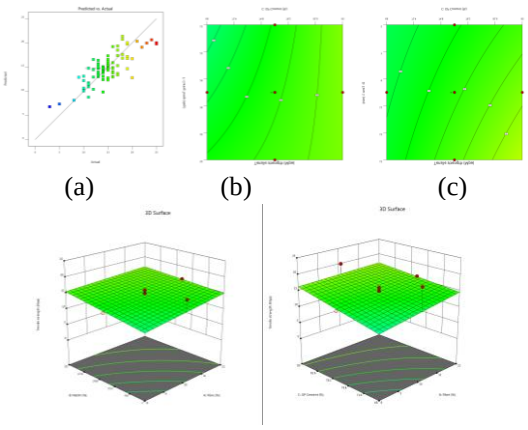

(a) (b) (c)

(d) (e)

Figure 3. Fit summary, 2d and 3D Surface Responses for Tensile Strength

Figure 3(a) depicts the actual regression model of tensile strength due to variations in cement percentage, curing temperature, mixing times, fibre concentration and alkali concentration.

Figure 3(b) shows the variation of tensile strength with actual variations of curing temperature and cement. Increases in temperature up to 50 degrees, results in a

corresponding increase in tensile strength above that the tensile strength begins to be negatively affected. Increases in temperature of up to 85% results in an increase in the tensile strength of the brick due to the increased impact of the cement bonding nature in the brick matrix. Cement percentages below 68% results in reduced cement bonding which leads to reduced tensile strengths.

Figure 3(c) shows the impact of variations in cement and mixing times on tensile strength. Increases of mixing times up to 15 minutes for the slow mixing and 35 minutes high speed mixing will result in optimized tensile strength of 25 Mpa. Further increases in mixing time result in a negative impact on the tensile strength due to an undesirable laminar floor in the fibres.

Figure 3(d) shows the 3d variations of tensile strength due to variations in fibre and NaOH. 11.99% of fibre is required together with 19.99% NaOH solution to achieve an optimized strength.

Figure 3(e) shows variations in tensile strength with variations of fibre and cement. 11.99% of fibre mixed with 83.88% cement is required to achieve an optimized strength.

4.2 Fit Summary Response 3: Thermal resistance

The fit summary for thermal response identifies the linear model as the best supported description, with a sequential p-value below 0.0001, an adjusted R-squared of 0.3118 and a positive predicted R-squared of 0.2368, while the higher-order models did not improve the prediction (Table 4). The fitted equation, given below, shows that thermal expansion decreases with increasing fibre content (factor A) and geopolymer cement content (factor C), confirming that a denser, more highly bonded matrix is more dimensionally stable when heated.

Table 4. Fit Summary for Response 3: Thermal Resistance

Linear	< 0.0001	0.4182	0.3118	0.2368
2FI	0.2319	0.4597	0.3482	0.0756
Quadratic	0.5021	0.4493	0.3420	-0.0148
Cubic	0.7627	0.3307	0.2623	-4.3228

Final Equation in Terms of Coded Factors

$$\begin{aligned} &Thermal\ Resistance \\ &= +0.8627 - 0.1295A\ - 0.0589B - 0.1709C \\ &- 0.0859D + 0.0411E \\ &- 0.0526F \end{aligned} \quad (4)$$

The equation in terms of coded factors can be used to make predictions about the response for given levels of each factor. By default, the high levels of the factors are coded as +1 and the low levels are coded as -1. The coded equation is useful for identifying the relative impact of the factors by comparing the factor coefficients.

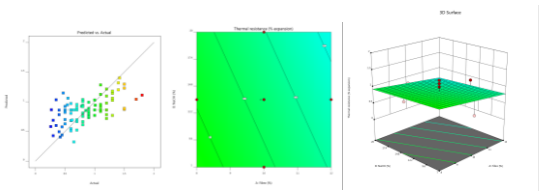

(a) (b) (c)

Figure 4(a) shows the response curve of variations of thermal in thermal resistance with variations in fibre and NaOH.

Figure 4(b) shows 2d responses of thermal resistance with variations in fibre and NaOH. The response curves show that optimum thermal resistance is obtained when fibre increases up to 11.9% and NaOH increases up to 19.9%. Higher levels of NaOH above 19.9% result in reduced strengths due to the corresponding decrease in bonding strengths achieved due to rapid setting.

Figure 4(c) Optimum strength of thermal resistance is obtained when 11.99% of fibre is mixed with 19.99% of NaOH.

4.3 Fit Summary Response 4: Acid Resistance

Final Equation in Terms of Coded Factors

$$\begin{aligned} &Acid\ Resistance \\ &= +77.31 + 4.92A + 6.72B + 11.71C + 3.70D \\ &- 0.1030E + 2.17F - 2.53AB - 3.10AC + 0.5344AD \\ &+ 3.14AE - 1.04AF + 4.15BC - 1.72BD - 1.54BE \\ &- 1.73BF + 2.85CD - 1.92CE - 2.92CF + 2.29DE \\ &+ 0.7937DF + 1.65EF - 8.62A2 - 6.12B2 \\ &+ 22.38C2 - 14.12D2 + 16.88E2 \\ &- 10.12F2 \end{aligned} \quad (5)$$

The equation in terms of coded factors can be used to make predictions about the response for given levels of each factor. By default, the high levels of the factors are coded as +1 and the low levels are coded as -1. The coded equation is useful for identifying the relative impact of the factors by comparing the factor coefficients. The fit summary for acid resistance is presented in Table 5.

Table 5. Predicted Acid Resistance R2 Values for Bricks after Chemical Attack

Source	**Sequential p-value**	**Lack of Fit p-value**	**Adjusted R^2**	**Predicted R^2**
Linear	< 0.0001	0.0058	0.4279	0.3724
2FI	0.0372	0.0102	0.513	0.3741
Quadratic	0.0313	0.0161	0.5735	0.2845
Cubic	0.0754	0.0339	0.6761	-9.491

Figure 5(a) shows the response of Acid Resistance to variations in NaOH and cement compositions. Optimized values of acid resistance are obtained when 19.99% NaOH is used and 83.88% cement is used. An optimum of 81.39% is achieved when 19.99% NaOH is used together with 83.88% cement achieving a corresponding weight loss of 0.019%.

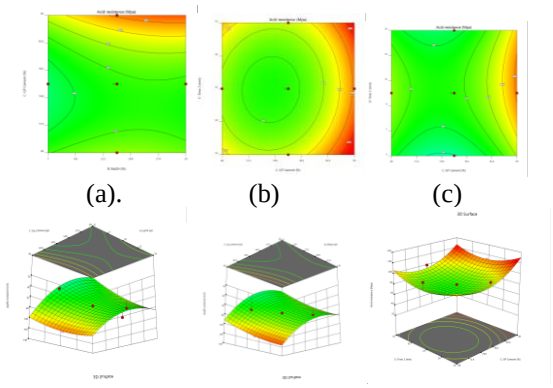

(a). (b) (c)

(d) (e) (f)

Figure 5. 2d and 3D Surface Responses for Acid Resistance

Figure 5(b) shows the variation of acid resistance with cement vs time 2 which is high speed mixing. Maximum strength is obtained when cement increases to 83.88% whilst the mixing time 2 is increased to 25 minutes. Any further increase in time does not result in any further increases in strength.

Figure 5(c) shows the variation of acid resistance to variations in cement and slow mixing time T1. Maximum strength is achieved when slow mixing time is increased to 15 minutes.

Figure 5(d) shows the variation of acid resistance to cement and fibre concentration variations. Maximum strength is obtained when 11.99% fibre is mixed with 83.88% cement.

Figure 5(e) 3d variation of acid resistance response to variations in NaOH and cement. Maximum strength is achieved when 19.99% NaOH is mixed with 83.88% cement.

Figure 5(f) Shows the 3d response of acid resistance to variations in time T2. Strength increases as time T2 increases to 25 minutes and cement increases to 83.88%.

4.4 Fit Summary Response 5: Weight Loss

The statistical fit for the weight loss response is summarized in Table 6.

Table 6. Response 5: Weight loss

Source	Sequential p-value	Lack of Fit p-value	Adjusted R^2	Predicted R^2
Linear	**0.0146**	**0.2541**	**0.1153**	**0.025**
2FI	0.2923	0.2732	0.1483	-0.1704
Quadratic	**0.0613**	**0.3425**	**0.2311**	**-0.1823**
Cubic	0.3169	0.3838	0.2915	-4.9342

Final Equation in Terms of Coded Factors

$$
\begin{aligned}
&Weight\ Loss \\
&= +0.5387 - 0.1212A - 0.0641B - 0.1929C \\
&+ 0.0023D - 0.0592E + 0.0333F - 0.0964AB \\
&+ 0.0545AC + 0.0214AD - 0.1127AE - 0.0095AF \\
&- 0.1177BC - 0.0395BD + 0.0739BE - 0.0261BF \\
&- 0.0930CD - 0.0189CE - 0.0802CF - 0.0152DE \\
&- 0.0170DF + 0.0252EF - 0.3153A2 - 0.0103B2 \\
&- 0.3403C2 + 0.0497D2 \quad - 0.3503E2 \\
&+ 0.9847F2 \qquad\qquad\qquad\qquad\qquad\qquad (6)
\end{aligned}
$$

The equation in terms of coded factors can be used to make predictions about the response for given levels of each factor. By default, the high levels of the factors are coded as +1 and the low levels are coded as -1. The coded equation is useful for identifying the relative impact of the factors by comparing the factor coefficients

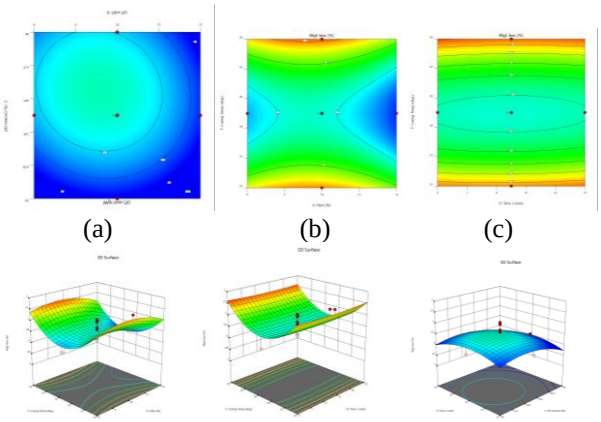

(a) (b) (c)

(d) (e) (f)

Figure 6. 2d and 3D Surface Responses for Weight Loss

Figure 6(a) shows 2d variations of weight loss with cement and fibre variations. Increases in fibre up to 11.99% with cement of up to 83.88% produces optimized results, further increases of fibre concentration result in increased weight losses due to the negative impact of higher fibre concentrations on the overall geopolymer mix.

Figure 6(b) shows the 2d variations of weight loss due to changes in fiber and curing temperature. The weight loss is optimized when fiber increases from 7% to 11.99% and the curing temperature is increased from 15 to 50 degrees. Higher curing temperatures results in stronger bonds which results in lower weight losses due to increased strength as curing time increases up to 50 degrees. Higher fiber concentrations results in higher weight loss values due to the reduced strength contributions when fiber goes above the optimum threshold values of 11.99%.

Figure 6(c) Shows the relationship between weight loss and time T1 against curing temperature. Lower values of T1 below 5 minutes result in inadequate mixing.

Optimum mixing times required for T1 is 15 minutes with a corresponding maximum temperature of 50 degrees.

Figure 6(d) Shows 3d response of fiber and curing time. Maximum weight loss is achieved when fiber concentration is low at 5% and curing temperature is also low at 15 degrees. This shows the lower end of the 3d response curve. High weight loss values are also recorded when fiber goes above 12% and curing temperature goes above 50 degrees.

Figure 6(e) Shows the relationship between weight loss with variations in curing temperature and mixing time T1. Lower curing temperatures and low initial mixing times T1 result in high weight losses as the bonding is not adequately developed. Low weight losses are achieved when curing temperatures of 50 degrees is mixed with an initial curing time T1 of 15 minutes.

Figure 6(f) shows the relationship between weight loss and variations between cement and high speed mixing time (T2). Increases in cement of up to 83.88% results in reduced weight losses and increases in time T2 from 15 to 35 minutes results in increases of time T2 to 23.99 minutes causes a reduction in weight loss. Increases of time T2 above 23.99 minutes causes an undesirable laminar orientation which causes reduced strength.

4.5 Fit Summary Response 6: Comprehensive Strength

The quadratic model gave the best representation of compressive strength, as shown in Table 7.

Table 7. Fit Summary for Response 6: Compressive Strength

Source	Sequential p-value	Lack of Fit p-value	Adjusted R^2	Predicted R^2
Linear	< 0.0001	0.0053	0.4255	0.3676
2FI	0.0250	0.0100	0.5207	0.3739
Quadratic	0.0225	0.0167	0.7386	0.3200
Cubic	0.0839	0.0335	0.6819	-9.1338

The quadratic model gave the best representation of compressive strength, raising the adjusted R-squared to 0.7386 with a sequential p-value of 0.0225, a clear advance on the linear (0.4255) and two-factor interaction (0.5207) models, while the cubic model was aliased. The large positive quadratic coefficient on the geopolymer cement content (factor C) confirms that strength rises steeply with binder content before the contribution levels off, which is consistent with the optimisation discussed below.

Final Equation in Terms of Coded Factors

$$\begin{aligned} &Compressive\ Strength \\ &= +78.41 + 4.68A + 7.02B + 11.45C + 3.56D \\ &- 0.3030E + 2.17F - 2.77AB - 3.05AC + 0.5469AD \\ &+ 3.27AE - 0.9531AF + 4.11BC - 1.80BD \\ &- 1.58BE - 1.92BF + 2.92CD - 1.61CE - 2.83CF \\ &+ 2.55DE + 0.8281DF + 1.67EF - 7.53A2 - 8.53B2 \\ &+ 22.97C2 - 13.53D2 + 16.97E2 \\ &- 9.53F2 \end{aligned} \quad (7)$$

The equation in terms of coded factors can be used to make predictions about the response for given levels of each factor. By default, the high levels of the factors are coded as +1 and the low levels are coded as -1. The coded equation is useful for identifying the relative impact of the factors by comparing the factor coefficients.

5. SUMMARY OF RESULTS

Optimised Result

Figure 7 shows the summary of the optimised experimental results.

Fibre Content

From the above optimised result, an increase in chrysotile asbestos fibre content was found to result in an increase in compressive and tensile strengths up to a value of 11.99% fibre content. This is mainly due to the positive reinforcement effect of the fibres on the finished product. The random dispersion of these fibres in the finished product results in some fibres providing their reinforcement effect laterally whist some provide their reinforcement effect in a perpendicular direction. The shorter fibres provide this perpendicular reinforcement mostly whilst the longer fibres provide the lateral reinforcement. As the fibre content continues to increase the longer fibres then also increase their orientation in the longitudinal direction of the product. The resultant strength then starts to diminish as increased slip between the fibres and the cement increases under a compressive force.

Alkali Content (NaOH)

The alkali acts as an activator of the geopolymer reactions that take place as the alumina-silicate bonds are formed. The strength of the finished geopolymer product was seen to increase with an increase of sodium hydroxide percentage up to 20% of alkali. Above this percentage the excess alkali which is present results in reduced strengths as no aluminium and silica molecules are available to react with the excess oxygen molecules provided by the hydroxide component of the alkali. This results in the creation of weaker bonds and production of excess water. It should be noted that the geopolymer reaction results in the production of water as a by-product as water of hydration is removed from the raw materials as they react.

Geopolymer Cement

Acid resistance, compressive and tensile strengths increased with an increase in geopolymer cement content. This was true up to 83.88%. Beyond this value the contribution of geopolymer cement to the finished product characteristics became less due to the reduced effect of the contribution of the reinforcing characteristics of the chrysotile asbestos fibre. The fibre mainly provides the reinforcement characteristics that result in increased tensile and compressive strengths. The major contribution is mainly on the acid resistance, tensile strength and thermal resistance properties due to an increase in improved flexural strength.

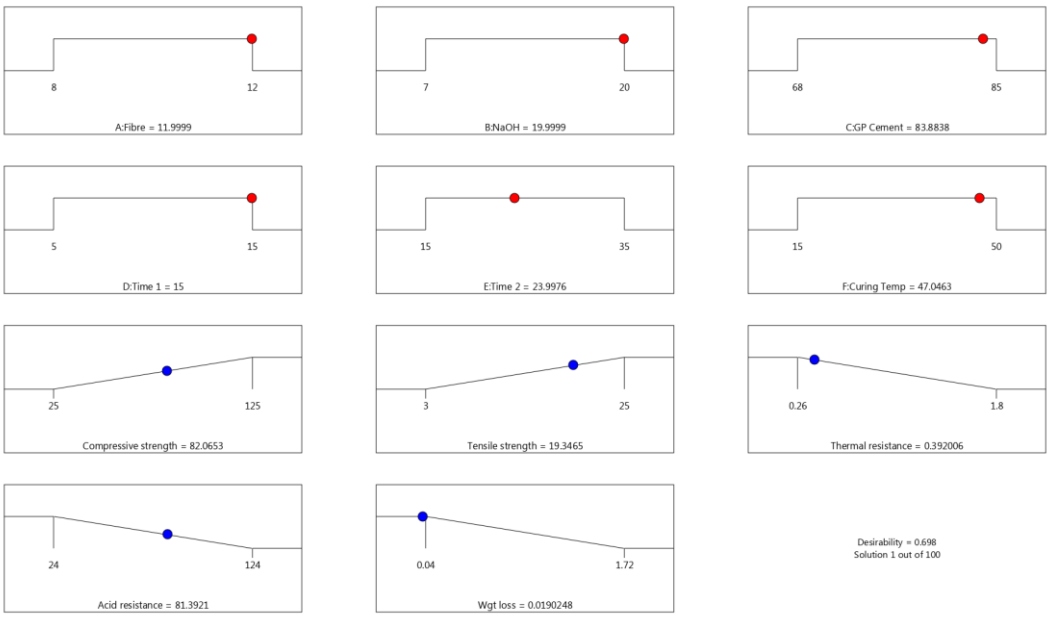

Figure 7. Experimental Results Summary

Initial Mixing Time

An initial mixing time of 15 minutes was desired. This was the maximum recommended value. The initial slow speed mixing at approximately 30 revolutions per minute of the geopolymer materials enables the initial geopolymer reactions to start taking place in the presence of the one molar solution of sodium hydroxide. As the mixing continues the paste slowly changes from dry to semi dry. When this semi dry state is achieved the geopolymer mixer will be ready for the next process.

Final Mixing Time

When the geopolymer paste is now semi dry, the high speed mixing is then initiated. This involves mixing at a mixer speed of 980 revolutions per minute. The best results were obtained after mixing for 24 minutes. Water of hydration is removed from the solid particles as the mixing is taking place. This water then appears as excess water when the paste is allowed to settle.

Curing Temperature

The chrysotile asbestos reinforced geopolymer paste that is produced is then placed in the brick forming machine. Special templates with the various required brick sizes are then used. The selected brick profile for this research is shown in Figure 8.

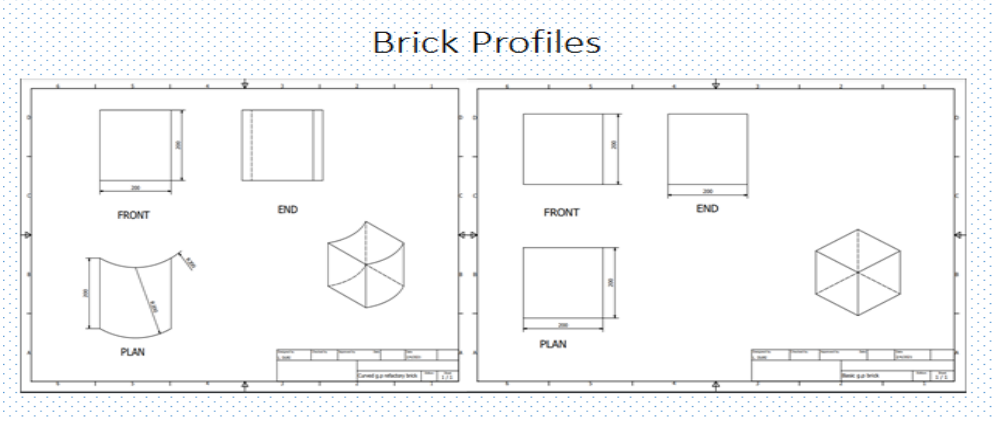

Figure 8. Refractory Brick Design

Two profiles were done. One with a curved surface for use in curved profiles at corners and bends, and one with a normal straight surface. The data used in this research was derived from the straight face brick profiles shown above. The optimum curing temperature was found to be 47 degrees Celsius.

5.1. Summary of Optimised Results

From the above optimised result, a compressive strength of 82MPA and a tensile strength of 19.3MPA were achieved. This was obtained together with a product thermal resistance of 0.39% in expansion, an acid resistance of 83MPA compressive strength after acid attack and a weight loss of 0.019% after acid attack. It was observed that the compressive strength increased as the percentage of geopolymer cement was increased. This was due to the increased bonding effect introduced by the additional geopolymer cement within the chrysotile asbestos reinforcement. This phenomenon reached a peak position after 83 % of the geopolymer cement binder material was added. Additional cement content above 83% resulted in a reduction in the amount of chrysotile asbestos fibre in the mixture. This optimum fibre content was found to be 11.99 %. An alkali activator of 19.99% of a 1M NaOH solution was required to achieve the optimum results. This facilitated the initiation of the geopolymer reaction at room temperature. When the mixing analysis was done, a two staged mixing process was found to achieve the best result. First a slow speed mixing of the chrysotile asbestos fibre at mixer speed of 30 revolutions per minute for 15 minutes and then followed by a high-speed mixing at 980 revolutions per minute for 24 minutes. This allowed optimum distribution of the fibre within the paste and also allowed the geopolymer reactions to form the alumina- silicate bonds to occur. This reinforced liquid geopolymer product was then poured into a brick preform allowed to set. It was then pressed out and cured at an optimum temperature of 47 degrees Celsius. The compressive strength of the chrysotile asbestos reinforced geopolymer material reduced to 81.3 MPA from 83.88 MPa after it was exposed to acid attack. This was caused by the slight decrease in weight after the surface had been attacked by the acidic reactions of 0.019%. The material was able to resist the attack from all types of acids mainly due to the superior strength of the Silica- Alumina-Oxygen bond. When the reinforced product was subjected to thermal heating, an expansion of 0.39% was observed which indicated at very small change in product dimension.

The fitted response surface models are mutually consistent and explain why these optimum settings emerge. Across the compressive strength, tensile strength and acid resistance models the geopolymer cement content (factor C) carries the largest positive linear coefficient, at +11.45, +1.97 and +11.71 respectively, while its quadratic term is strongly positive in the strength and acid models, at roughly +22 to +23. This combination of a positive linear and positive quadratic term reproduces the observed behaviour in which strength climbs with binder content up to about 83 per cent and then yields diminishing returns as the available fibre reinforcement is displaced. The alkali concentration (factor B) is the second most influential factor, and its sign reverses once the activator exceeds the stoichiometric demand of the available alumina and silica, which is consistent with the loss of strength observed beyond about 20 per cent NaOH.

Linking the two experimental programmes, the grinding optimisation of Experiment 1 underpins the brick performance reported in Experiment 2. The high-fineness, low-residue feed selected from the surface area and residue models provides the reactive surface needed for rapid alumina-silicate dissolution, so that the geopolymer reaction can be initiated at room temperature with only a 1 M activator and completed at a curing temperature of 47 degrees Celsius. This is appreciably lower than the minimum of about 57 degrees Celsius typically required for asbestos cement pipe, and the resulting brick retained 81.3 MPa of its compressive strength after acid attack at pH 1 with a mass loss of only 0.019 per cent. Taken together, the optimised feed and mix design yield a reinforced geopolymer brick whose mechanical and chemical performance exceeds that of conventional limestone-based cement products, while remaining economical to produce.

6. RECOMMENDATIONS

The Authors recommended that Chrysotile asbestos reinforced geopolymer materials exhibit superior Physical and Chemical characteristics when compared to the limestone-based cement materials. They also noted that asbestos reinforced geopolymer cement materials can be used effectively in corrosive environments. The authors further noted that asbestos reinforced cement materials can be produced using lower curing temperatures, at 47 degrees as compared to asbestos cement pipes which are cured at 57 degrees Celsius minimum. They also noted that Chrysotile Asbestos fibre furnish optimisation can be done to further improve on the compressive and tensile strength development.

7. CONCLUSIONS

From the research done it can be safely concluded that Chrysotile asbestos reinforced geopolymer cements can be used in special applications that require high mechanical and chemical strength properties such as in refractories used in very corrosive environments. Chrysotile asbestos reinforced geopolymer cement composite materials can be used in applications where high thermal resistance is required such as spacecraft casings and insulation materials. The authors further concluded that due to the high thermal flash point of both the geopolymer cement and the chrysotile asbestos fibre materials, they can be used in applications where

protection from fires (fire shields) is required. These include use in aircraft cabin materials, fire aprons etc.

Acknowledgment:
I would like to express my sincere gratitude to my three supervisors, Dr Rajesh Aurora, Dr Naveen BP and Dr Rajesh Goyal, Associate Professors at Amity University School of Engineering and Dean Research and PhD programs NICMAR Pune India. The encouragement they gave me at a time when sometimes I felt like giving up is most appreciated. Their support and guidance have significantly contributed to the completion of this research work. I would also like to acknowledge contributions from Dr Shiv Sharma and Professor R. Marlik, Dr Eng. Q.C. Kanhukamwe, Dr Rungano Karimanzira, Professor Tagwira, and Eng. Trust Marongedze for the mentoring, support and encouragement that they provided during the course of my research. My special thanks go to my wife Rudo Duri, my children Zvikomborero Claire, Tinotenda and Simbarashe Brendon Duri for standing by me and for being patient, supportive and pushing me to go all the way and finish the research work. I will forever be grateful to all these people. Lastly, I would want to thank God the Almighty for the wisdom, guidance, security and direction that he continues to provide.

References:

Abd Elaty, M. A. A. (2014). Compressive strength prediction of Portland cement concrete with age using a new model. *HBRC Journal*, *10*(2), 145–155. https://doi.org/10.1016/j.hbrcj.2013.09.005

Davidovits, J. (1991). Geopolymers—Inorganic polymeric new materials. *Journal of Thermal Analysis*, *37*(8), 1633–1656.

Duxson, P., Lukey, G. C., & Van Deventer, J. S. J. (2006). Thermal conductivity of metakaolin geopolymers used as a first approximation for determining gel interconnectivity. *Industrial & Engineering Chemistry Research*, *45*(23), 7781–7788.

Lyon, R. E., Balaguru, P. N., Foden, A., Sorathia, U., Davidovits, J., & Davidovics, M. (1997). Fire resistant aluminosilicate composites. *Fire and Materials*, *21*(2), 67–73.

Palomo, A., Blanco-Varela, M. T., Granizo, M. L., Puertas, F., Vázquez, T., & Grutzeck, M. W. (1999). Chemical stability of cementitious materials based on metakaolin. *Cement and Concrete Research*, *29*(7), 997–1004.

Provis, J. L., & Van Deventer, J. S. J. (Eds.). (2009). *Geopolymers: Structures, processing, properties and industrial applications*. Elsevier.

Wang, H., Li, H., & Yan, F. (2005). Reduction in wear of metakaolinite-based geopolymer composite through filling of PTFE. *Wear*, *258*(10), 1562–1566.

Yeh, C. (2006). Generalization of strength versus water–cementitious ratio relationship to age. *Cement and Concrete Research*, *36*(10), 1865–1873. https://doi.org/10.1016/j.cemconres.2006.04.027

Zvikomborero Lazarus Duri
ASET, Amity University
Haryana,
India
lazarus@rulethu.com
ORCID 0009-0008-5868-1079

Rajesh Arora
ASET, Amity University
Haryana,
India
rarora64@ggn.amity.edu
ORCID 0000-0001-9234-4115

Naveen B.P.
ASET, Amity University
Haryana,
India
bp.naveen864@gmail.com

Q.C. Kanhukamwe
Harare Institute of Technology,
Harare,
Zimbabwe
qckanhukamwe@hit.ac.zw

Appendix

Table 3. Sample of Table of Experimental Results

		Factor 1	Factor 2	Factor 3	Factor 4	Factor 5	Factor 6	Response 1	Response 2	Response 3	Response 4	Response 5
std	Run	A: Fibre	B: NaOH	C: Geopolymer Cement	D: Time 1	E: Time 2	F: Curing Temperature	Compressive Strength 20 to 125	Tensile 3 to 25	Thermal Response	Acid Resistance in acid solution pH of 1	Mass in Kg
		%	%	%	Min	Min		Mpa	Mpa	% Expansion	Comprehensive Strength in %	% Weight los
9	1	8	7	68	15	15	15	50	5	0.47	49.5	0.1
17	2	8	7	68	5	35	15	25	3	1.42	24	0.12
8	3	12	20	85	5	15	15	100	24	0.35	99.3	0.07
58	4	12	7	68	15	35	50	120	25	0.27	118	0.09
69	5	10	13.5	69	10	25	32.5	105	20	0.35	103	0.09
16	6	12	20	85	15	15	15	110	18	0.3	109	0.08
23	7	8	20	85	5	35	15	105	19	1.01	104	0.06
52	8	12	20	68	5	35	50	96	15	0.8	95	0.09
73	9	10	13.5	76.5	10	15	32.5	103	16	0.5	103	0.04
2	10	12	7	68	5	15	15	76	14	0.55	75	0.09
47	11	8	20	85	15	15	50	114	23	0.26	112	0.07
56	12	12	20	85	5	35	50	75	13	0.43	73	0.09
53	13	8	7	85	5	35	50	60	11	0.7	59	0.1
71	14	10	13.5	76.5	5	25	32.5	80	14	0.54	78	0.08
46	15	12	7	85	15	15	50	67	12	0.45	66	0.1
63	16	8	20	85	15	35	50	108	19	0.9	106	0.23
64	17	12	20	85	15	35	50	125	25	0.42	124	0.05
48	18	12	20	85	15	15	50	113	22	0.65	112	0.06